PHYSICAL REVIEW B VOLUME 23, NUMBER 12 15 JUNE 1981

Possible configurational model for hydrogen in amorphous Si:H. An exodiffusion study

K. Zellama, P. Germain, and S. Squelard
Groupe de Physique des Solides de l'Ecole Normale Supérieure, Université Paris 7, Tour 23, 2 place Jussieu, 75221 Paris Cedex 05, France

B. Bourdon
Laboratoire de Marcoussis, Centre de Recherches, Compagnie Générale d'Electricité, Departement Matériaux, Route de Nozay, 91460 Marcoussis, France

J. Fontenille and R. Danielou
Département de Physique Fondamentale, Commissariat á l'Energie Atomique, Centre d'Etudes Nucléaires de Grenoble, 85 X, 38041 Grenoble, France

(Received 15 July 1980)

The kinetic hydrogen exodiffusion and its temperature dependence in amorphous silicon prepared by glow discharge of silane has been studied using conductivity, electron paramagnetic resonance, $^{11}B \rightarrow \alpha$ nuclear reaction, and infrared absorption measurements. Comparison of the results obtained with these techniques shows the existence of two principal stages in the H exodiffusion. The hydrogen evolution for $T \leq 500$ °C is controlled by a diffusion process with a diffusion coefficient D. D is thermally activated; $D = D_o\, e^{-E_D/k_BT}$ with $D_o = 4.7 \times 10^{-3}$ cm^2/s^{-1} and $E_D = 1.5$ eV (where k_B is the Boltzmann constant). The hydrogen evolution above 500 °C is controlled by a first-order process. The activation enthalpy and entropy are, respectively, $\Delta H_2 = 3.4$ eV and $\Delta S_2 = 7.8k_B$. The fact that the EPR signal appears during the second stage and that ΔH_2 is equal to the Si-H bound energy is a direct evidence that EPR signal is associated with the breaking of this bond. We then deduce an exodiffusion model assuming that hydrogen atoms can be bound in two sorts of centers. A possible configuration of H occupying such sites in the amorphous network is proposed.

I. INTRODUCTION

The physical properties of hydrogenated amorphous silicon prepared by glow discharge of silane (a-Si-H) have been extensively studied by many research groups. It has electrical and optical properties which evaporated amorphous silicon do not have.[1-3] We admit that hydrogen atoms saturate broken bonds in the network (it apparently lowers the electrically active states associated with these bondings to the valence band), for there are 10^{16} cm^{-3} dangling bonds instead of 10^{19} cm^{-3} in the evaporated material.[4,5] In addition, a-Si-H can be easily doped.[6,7] In fact, the hydrogen concentration in the a-Si-H material is much larger than the dangling-bond concentration measured in the evaporated amorphous silicon.[4] The hydrogen concentration ranges from 10 to 16 at. % (2×10^{21} cm^{-3}) for films deposited at high substrate temperature (450 °C).[8,9] We can then ask the following questions: Where can the hydrogen be in the amorphous film? What is the hydrogen quantity necessary to saturate the broken bonds?

Thus the study of the exodiffusion (or incorporation) of hydrogen in amorphous silicon is very interesting.[10-24] We can control the hydrogen evolution and leave in the sample the necessary quantity of hydrogen to saturate the broken bonds.

Many research groups have studied the post-hydrogenation and the exodiffusion of hydrogen in amorphous silicon as a function of annealing temperature. Various techniques have been used: measurement of the rate of H_2 desorption,[10-12,18] infrared absorption[12-17,20,21] (ir), electrical conductivity,[13,14] optical gap,[17,21] electron paramagnetic resonance[13,14,18,19,21] (EPR), secondary-ion mass spectroscopy[20,22] (SIMS), photoluminescence,[12,14,18,23] nuclear reaction analysis,[13-15,17] mass spectroscopy, and reflection high-energy-electron diffraction (RHEED) measurements.[24] Some authors observe two stages of annealing.[10,12,16,18,21,24-26] The majority of these authors have found SiH, SiH_2, and SiH_3 or $(SiH_2)_n$ complexes in their amorphous layers. Oguz *et al.*[11,12] and Deneuville *et al.*[17] observed a hydrogen which is infrared inactive; consequently this hydrogen is not covalently bonded to a silicon site. Brodsky *et al.*[10] and McMillan *et al.*[26] have measured the mean hydrogen atomic concentration $\bar{C}$ during exodiffusion of H. Other authors have made a correlation between $\bar{C}$ and physical parameters during the exodiffusion of H.[11,12,17,18,21,23,25] Some of them obtained $\bar{C}$ by measuring the rate of evolution of H,[10-12,18,23,25,26] others use nuclear reaction measurement[17] or mass spectroscopy.[21] None of these authors have made nuclear profiling measurements giving the local hydrogen concentration $C(x)$ versus the depth x. These measurements are the only way to show clearly the diffusion mechanism of H. Only a few research groups deduce mechanism and/or orders of reaction and their activation energies.[10-12,18,25,26] Brodsky *et al.*,[10] by measuring the hydrogen evolution

rate, studied several kinds of samples prepared by glow-discharge decomposition of silane, particularly those deposited at low pressure and high substrate temperature (containing only Si-H complexes). They found that the exodiffusion takes place in two annealing stages occurring, respectively, around 420 and 495 °C. Both correspond to a second-order process with activation enthalpies of 1.95 to 2.17 eV. McMillan *et al.*[26] studied amorphous silicon prepared by glow-discharge decomposition of silane; using the same technique, they found the two annealing stages occurring, respectively, around 350 and 580 °C. They found that the first is due to the departure of hydrogen coming from SiH_2 complexes and is associated with a first-order process with an activation enthalpy of around 1 to 1.4 eV. The second stage is due to the departure of H coming from SiH complexes. It seems to be associated with a first-order process with an activation enthalpy of 0.6 to 0.88 eV. Biegelsen *et al.*,[18,25] using glow-discharge deposited silicon samples prepared in various conditions, correlated measurements of the rate of hydrogen evolution with luminescence and EPR measurements. They observed a decrease of the spin concentration versus annealing temperature for temperature ranging from room temperature to 300 °C. This stage is associated with an activation enthalpy of 0.5 eV. They showed that a diffusion effect exists, using samples of various thicknesses and containing only SiH complexes. Finally, Oguz *et al.*,[11,12] using reactively sputtered amorphous films, correlated infrared and photoluminescence measurements with hydrogen evolution rate measurements. They found two annealing stages of exodiffusion taking place, respectively, at 300 and 600 °C. The first stage corresponds to the departure of hydrogen which is infrared inactive. This stage is associated with a first-order process with an activation enthalpy of 0.4 eV. This departure is not diffusion limited. The second stage is associated with an activation enthalpy of 1.6 eV. This value is equal to the activation enthalpy of desorption of hydrogen of crystalline silicon (111) surfaces. Oguz *et al.* observed a non-diffusion-limited process (desorption), whereas Brodsky *et al.* expected and Biegelson *et al.* showed that in their samples, diffusion is one of the limiting processes. The above research groups[10,15-18,21,23-26] either interpreted their results on exodiffusion of H quantitatively but gave scattered values of the activation energies for the two annealing stages, or they did not interpret their results quantitatively. This seems to be because they measured $\overline{C}$ instead of $C(x)$ and/or their samples often contained hydrogen occupying various sites [SiH, SiH_2, SiH_3, $(SiH_2)_n$, and infrared-inactive hydrogen]. It is difficult in such conditions to obtain simple kinetics, and consequently it is not possible to obtain activation energies for elementary processes. Deneuville *et al.*[17] noticed that there is a dynamical equilibrium between hydrogen in the configuration SiH, SiH_2, and SiH_3.

Meanwhile, other research groups have clearly shown the existence of a diffusion stage.[13,20,22] Carlson *et al.*[22] measured the diffusion of deuterium in hydrogenated amorphous silicon prepared by glow discharge of silane, using SIMS. They found a diffusion coefficient D, with an activation energy of 1.53 eV. Dieumegard *et al.*[20] studied the diffusion of deuterium in amorphous implanted silicon films and evaporated amorphous silicon. Using SIMS and nuclear reaction profiling measurements, they found a diffusion coefficient which is in good agreement with the Carlson results. Sol *et al.*,[13] studying post-hydrogenation of amorphous silicon films obtained by chemical vapor decomposition of silane (CVD), obtained results of D in good agreement with the above results.[20,22] These results are correlated with EPR and conductivity measurements. Thomas *et al.*[27] studied post-hydrogenation of evaporated amorphous silicon films prepared in high-purity conditions and high substrate temperature.[4] Their values of D are in good agreement with those of Refs. 13, 20, and 22.

The aim of this study is to present experimental results for the exodiffusion of H obtained in a simple material which does not contain SiH_2, SiH_3, and $(SiH_2)_n$ complexes. We use experimental techniques (EPR, ir, and conductivity) which give complementary information concerning the behavior of the amorphous material. We correlate these physical measurements with nuclear reaction profiling which provides $C(x)$. We then interpret our results using a kinetic model of exodiffusion. This allows us to propose a possible model for configurations of H in the amorphous network and to determine the amount of hydrogen necessary to saturate the broken bonds.

II. EXPERIMENTAL RESULTS

A. Sample preparation

Amorphous silicon films have been prepared by glow-discharge decomposition of silane, deposited on sintered alumina or quartz or silicon substrates. EPR and nuclear reaction profiling measurements have been made using samples deposited on suprasil quartz substrates (the 2 and 3 series). Most of the conductivity measurements were made on amorphous silicon deposited on

TABLE I. Experimental conditions for sample depositions.

Series	Experiments	Substrate	Substrate temperature during glow-discharge deposition (°C)	Thickness (Å)	Residual pressure (10^{-2} Torr)	rf power (W)	Sample tension (V)	Target tension (V)
1[a]	Electrical conductivity, isochronal and isothermal runs	Sintered alumina	420	6000	1.6	80	0	−450
2	Analysis by nuclear reaction	Quartz "suprasil"	450	8000	2.2	70	0	−400
3	Analysis by nuclear reaction, EPR, and electrical conductivity	Quartz "suprasil"	450	8000	2.2	70	0	−400
4	Analysis by ir absorption	Single crystal silicon	450	6600	1.6	60	0	−400

[a] Series 1 and 2 were in the same run.

sintered alumina substrate (the 1 series), few measurements being made on the 3 series. ir measurements were made on amorphous samples deposited on silicon single-crystal substrate (the 4 series). The preparation conditions detailed in Ref. 28 are summarized in Table I. In order to minimize the concentration of SiH_2 and SiH_3 complexes[8,1,9] a high deposition temperature (420–450 °C) has been maintained. Thickness measurements were made with a Talystep (±0.02 μm).

B. Results

1. Electrical conductivity measurements

Electrical conductivity (σ) measurements were made using a Keithley 610C electrometer with a relative error less than 10%; we use a planar configuration, with contact electrodes made by pressing with platinum foil. The annealing was done in an oven under argon atmosphere (stabilized at ±1 °C). A series of isochronal annealings (duration $\theta = 30$ min with temperature intervals of 20 °C) have been performed for temperatures ranging from 150 to 700 °C on samples of the 1 and 3 series. After each isochronal run, the sample temperature is decreased to 60 °C and the electrical resistance was measured. Figure 1 gives the plot of the electrical conductivity measured at 60 °C, $\sigma(\theta, T, 60\,°C)$, versus the maximum temperature of annealing T during the last

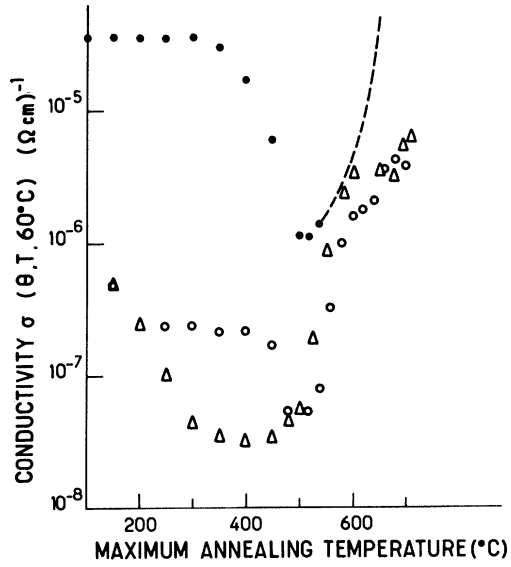

FIG. 1. Variation of the electrical conductivity σ measured at 60 °C versus annealing temperature during isochronal runs for various kind of silicon films: ○, glow-discharged amorphous silicon of the 3 series; △, glow-discharged amorphous silicon of the 1 series; ●, evaporated amorphous silicon film prepared in high-purity conditions (Ref. 4).

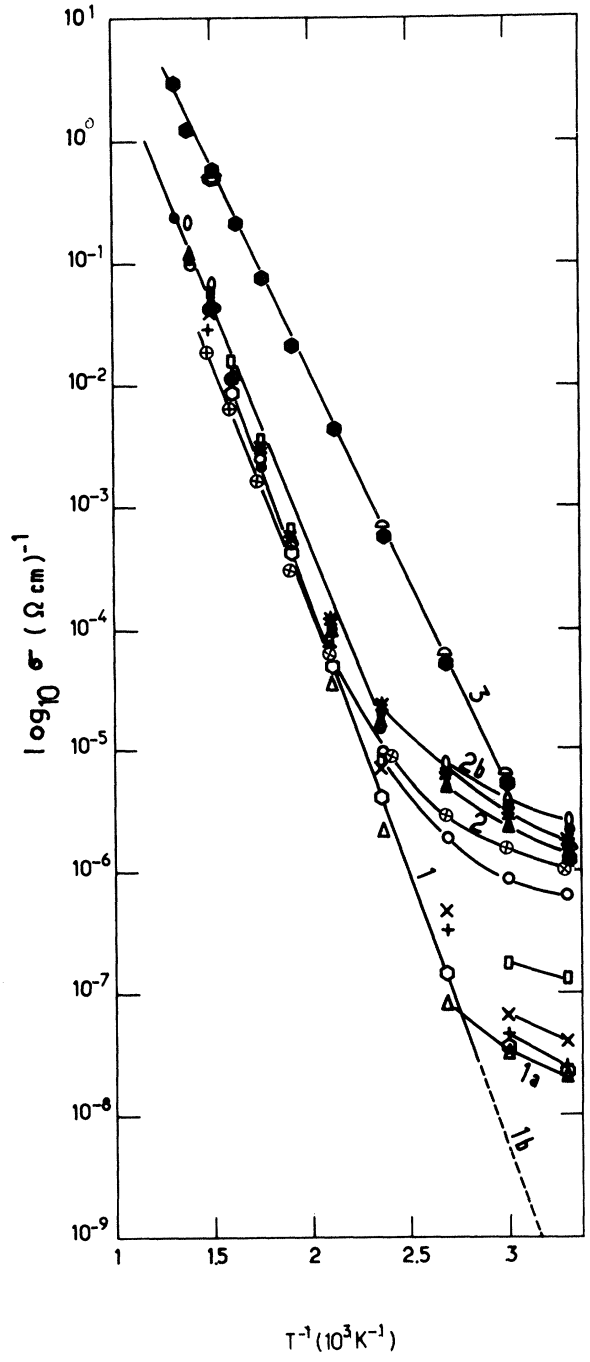

FIG. 2. Evolution of the behavior of the conductivity $\log_{10}\sigma$ versus reciprocal temperature $1000/T$ for one sample of the 1 series after each of the isochronal warm up presented in Fig. 1. After one annealing (30 min) at △, 400 °C; ⬯, 450 °C; +, 480 °C; ×, 500 °C; □, 520 °C; ○, 550 °C; ▲, 580 °C; ●, 600 °C; ⬮, 650 °C; *, 670 °C; ⬢, 690 °C; ⌓, 710 °C. ⊕, evaporated amorphous sample.

isochronal annealing. The temperature rise time is negligible compared with θ.

In Fig. 2 we plot $\log_{10}\sigma$ versus reciprocal temperature (limited to T, annealing temperature), measured during the temperature decrease after the isochronal anneal at temperature T. Other samples of the 1 series were isothermally annealed; the temperature of the sample was held at T for a time Δt, then decreased for measurement. Next the temperature is held again at T for Δt, and so on. We define $\sigma(t, T, 60\,°C)$ as being the electrical conductivity measured at 60 °C after an isothermal run of total duration t at temperature T. These studied samples are previously annealed at 450 °C for 30 min in order to get a thermal stability and to define a common initial state. $\sigma(450\,°C, 60\,°C)$ is the electrical conductivity measured at 60 °C after this initial anneal. We present in Fig. 3 $\sigma(450\,°C, 60\,°C)/\sigma(t, T, 60\,°C)$ versus annealing time t. The annealing temperature ranges from 500 to 540 °C. This particular choice of temperature (which corresponds to an annealing stage) will appear clear in the discussion.

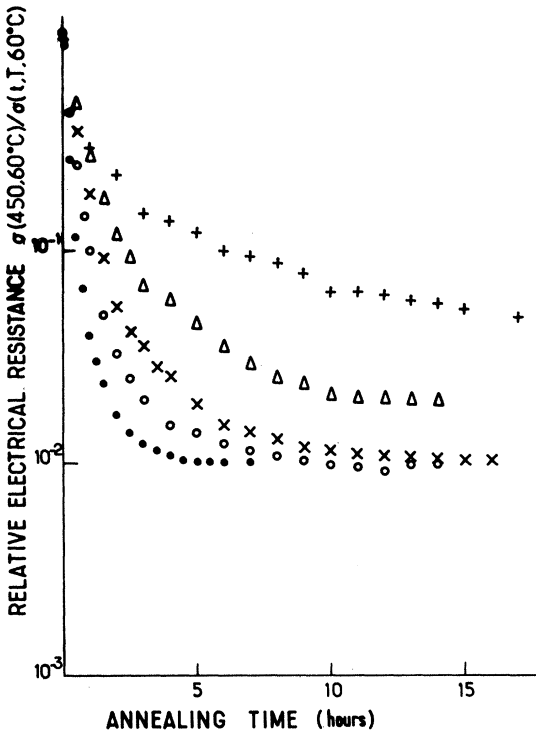

FIG. 3. Variation of $\sigma(450\,°C, 60\,°C)/\sigma(t, T, 60\,°C)$ (for samples of series 1) versus annealing time during isothermal runs at various temperatures: +, 500 °C; △, 510 °C; ×, 520 °C; ○, 530 °C; ●, 540 °C.

2. EPR measurements

EPR measurements have been performed on samples of the 3 series that were annealed for 30 min at a given temperature, ranging from 300 to 700 °C. The experimental conditions and some of the results have been reported in Ref. 19; spin density measurements are made at room temperature (≃20 °C). For calibration, an evaporated amorphous silicon sample prepared in high purity conditions and having a spin density of 3×10^{19} spins cm^{-3} (Ref. 27) is used. Figure 4 shows the mean spin density versus the annealing temperature.

3. Nuclear reaction profiling measurements

The same samples of the 3 series were also used for nuclear reaction profiling. The incident ^{11}B beam (2 MeV) interacts with hydrogen in the sample according to the nuclear reactions

$$^{11}B + {}^{1}H \rightarrow \alpha + {}^{8}Be \rightarrow \alpha + 2\alpha .$$

The depth resolution is about 400 Å. This technique is described in Refs. 29–32. Experimental excitation data, i.e., the number of counted α particles, are plotted versus the energy of the incident ions in Figs. 5 and 6.

4. Infrared absorption measurements

Infrared absorption measurements were made using a Perkin Elmer spectrometer (type 580) (with a relative error of 5% to 10%) on samples of the 4 series, annealed in the same way as samples of the 3 series. The wave vector (λ^{-1}) ranged from 500 to 2400 cm^{-1}. Figure 7 shows the infrared vibrational absorption spectrum of an unannealed hydrogenated amorphous silicon sample. The left-hand side of the figure (higher wave number) has been normalized to facilitate inspection of the 2000-cm^{-1} peak. The right-hand side was normalized to facilitate inspection of the 640-cm^{-1} peak.

In Fig. 8 we present the variation of the Si–H bond concentration $C_{SiH}(T)$ measured at room temperature after the annealing at T and deduced from the amplitude of the 2000-cm^{-1} peak versus annealing temperature. Using the Brodsky method,[33] one deduces an atomic concentration of Si–H bonds before annealing of 0.04. This calibration method may introduce error in the determination of this Si-H concentration; consequently this will be discussed in the conclusion section.

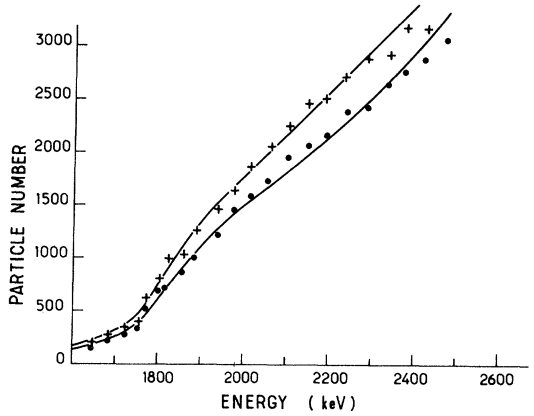

FIG. 5. Yield of the nuclear reaction from samples of the 3 series after annealing of 30 min at +, 400 °C; •, 460 °C. The solid lines have been obtained by a convolution process assuming a profile given by Eq. (1).

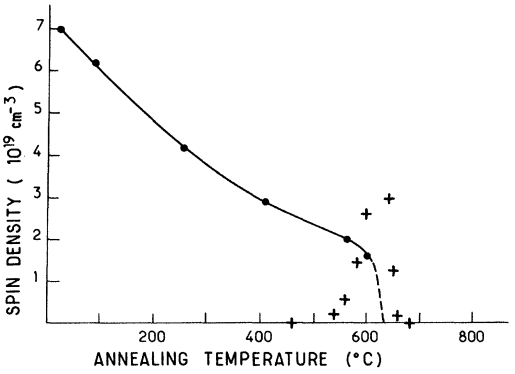

FIG. 4. Variation of the spin density versus annealing temperature for +, hydrogenated amorphous silicon of the 3 series. Each cross presents one sample annealed 30 min at a given temperature. •, one evaporated amorphous silicon film prepared in ultrahigh vacuum (Thomas, Ref. 4) after isochronal runs of durations of 2 h.

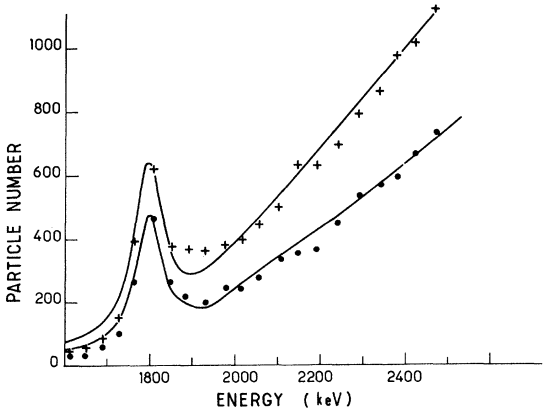

FIG. 6. Yield of the nuclear reaction from samples of series 3 after annealing of 30 min at +, 600 °C; •, 640 °C. The solid lines have been obtained by a convolution process assuming a profile given by Eq. (1) added with a surface peak.

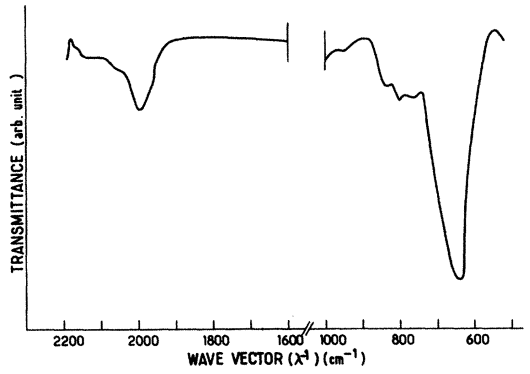

FIG. 7. ir spectra for an unannealed sample of series 4.

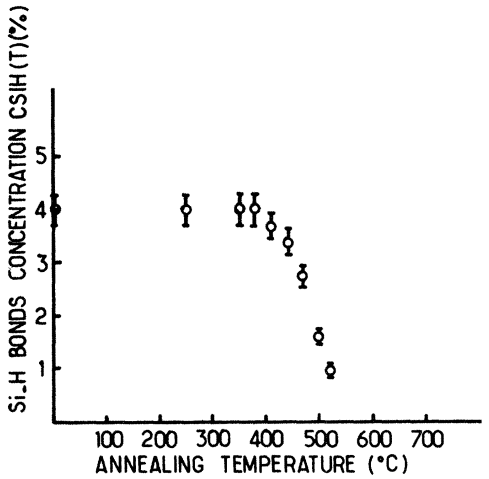

FIG. 8. Relative variation of the Si-H concentration obtained from ir measurements versus annealing temperature.

III. INTERPRETATION OF EXPERIMENTAL RESULTS

A. ir absorption

Many research groups and mainly Brodsky *et al.*[33] have characterized the different vibrational modes concerning the SiH, SiH_2, and SiH_3 complexes by infrared absorption measurements. They show that the 2000-cm^{-1} peak (stretching vibrations) and the 640-cm^{-1} peak (wagging vibrations) are associated with the SiH complex, while the SiH_2 and SiH_3 complexes correspond to the 2090- and 2120-cm^{-1} peaks (stretching vibrations) and the 890- and 850-cm^{-1} peaks (bending vibrations). Thus, the infrared spectrum presented in Fig. 7 shows that our unannealed amorphous hydrogenated silicon films contain mainly the Si-H complex. Figure 8 shows that the atomic concentration of the Si–H bond begins to decrease above 410 °C. It was not possible to measure Si-H concentration above 520 °C because of the sensitivity of the experimental method.

B. Electrical conductivity

The plot of $\sigma(\theta, T, 60\,^{\circ}C)$ vs T (Fig. 1) shows three annealing stages. The first stage corresponds to an annealing temperature ranging from 150 to 450 °C. The decrease in conductivity is possibly due to defect rearrangement. The behavior of the conductivity is different for samples of the 1 and 3 series, and both are quite different from the results for evaporated silicon prepared in high-purity conditions, plotted also in Fig. 1 for comparison. After the annealing at 450 °C, the extrapolation to room temperature of the intrinsic regime of $\log_{10}\sigma$ vs $1000/T$ deduced from our measurements, curve 1*b* in Fig. 2, is close to the conductivity reported by Spear and Le Comber[34] at room temperature on *a*-Si-H films. The high-temperature activation energy of σ is about 0.85 eV.

The second stage corresponds to temperature ranging from 450 to 640 °C. The important increase of $\sigma(\theta, T, 60\,^{\circ}C)$ is probably due to the variation of states in the gap. The variation $\log_{10}\sigma$ vs $1000/T$ changes very rapidly, and at the end of the stage, the conductivity of the sample behaves in a very similar manner to that of hydrogenless evaporated amorphous silicon films[4] also plotted (see curves 1, 1*a* and 2, 2*b* in Fig. 2). Thus the increase of $\sigma(\theta, T, 60\,^{\circ}C)$ for $450 < T < 640\,^{\circ}C$ is suggested to be due to the departure of hydrogen atoms leaving electrically active centers. We observe the same behavior of σ for samples of the 1 and 3 series. At the end of the stage, the high-temperature activation energy of σ (Fig. 2) is 0.8 eV. We note that this stage corresponds closely, but a little higher, to the stage observed in the ir results.

Finally, the third stage appears for $T > 640\,^{\circ}C$ with a new increase of σ (Fig. 1): It corresponds to crystallization. It has been studied extensively in Ref. 35, and shows that crystallization occurs at the same temperature for both samples of the 1 and 3 series. Figure 2 (curve 3) shows that at the end of the third stage, the high-temperature activation energy of σ is $Ec = 0.68$ eV, much greater than that for single-crystal silicon. This could be due to a residual concentration of hydrogen or to the presence of grain boundaries.

C. EPR results

Figure 4, which presents the variations of spin density versus annealing temperature, shows that for hydrogenless evaporated amorphous silicon[4] the spin density measured at room temperature decreases monotonically with increasing T. One

observes two stages: The first one occurs for temperature ranging from room temperature to 600 °C (corresponding to a binding recovery); the second one begins at 600 °C, which corresponds to crystallization. The hydrogenated amorphous silicon films have a completely different behavior. The spin density measured is zero for annealing temperatures below 500 °C. We observe an annealing stage (beginning at this temperature) for which the spin density increases rapidly with temperature. The spin density reaches a maximum value at 640 °C. This stage corresponds closely to the second annealing stage seen in conductivity. Then we observe the crystallization stage for $T > 640$ °C. This one corresponds to the third annealing stage seen in conductivity. At 600 °C the spin density of both samples is of the same order of magnitude. Apparently the annealing above 500 °C of hydrogenated amorphous silicon sample creates dangling bonds, suggesting that it is due to the departure of hydrogen. The stage of increasing of the spin density for $500 < T < 640$ °C has been studied elsewhere.[19] It has been shown that the increase of the spin density is controlled by a first-order process thermally activated with an activation energy of 3.4 eV (this will be recalled in the discussion section). This value is equal to the Si–H bond energy.[36]

D. Nuclear profiling

To extract the hydrogen profile $C(x)$ from the excitation data, we have used a convolution process.[29] We assume for the hydrogen profile the expression

$$C_{\text{expt}}(x) = C_p\left[1 - \frac{1}{G_A}\exp\left(-\frac{x}{S_p}\right)\right] \quad \text{for } T < 500\,^{\circ}\text{C}. \tag{1}$$

For $T > 500$ °C the hydrogen profile consists of a thin layer at the surface and a bulk distribution obeying Eq. (1). The fit of the excitation curve (shown as a solid line in Figs. 5 and 6) provides values of the parameters C_p, S_p, G_A for each sample of the 3 series. These values of parameters are given in Table II. We note that this experimental method[29] provides the absolute H concentration with an error less than 15% and the relative variations with a relative error of 5% to 10%. We use expression (1) because the expressions of $C_{\text{expt}}(x)$,

$$C_{\text{expt}}(x) = C', \tag{2}$$

$$C_{\text{expt}}(x) = C'' \operatorname{erf}\left(\frac{x}{2x_0}\right), \tag{3}$$

provide a less good fit with the excitation data; such a nuclear profiling method is sensitive to the whole hydrogen content. In Fig. 9 we plot the hydrogen concentration versus depth x deduced from Eq. (1) and Table II. The atomic concentration of H has been calculated assuming 4×10^{22} cm^{-3} atoms of silicon in the a-Si-H films. The surface hydrogen concentration peak corresponding to a negligible hydrogen content is not presented. The mean concentration of hydrogen is given by

$$\bar{C}_{\text{expt}} = \frac{1}{e}\int_0^e C_{\text{expt}}(x)dx, \tag{4}$$

TABLE II. Experimental values of C_p, S_p, G_A, CS, and SS according to Eq. (1) added with a Gaussian surface peak. CS and SS are, respectively, the surface H concentration and the width of the surface peak.

T (°C)	C_p (10^{10} μm^{-3})	S_p (μm)	G_A	CS (10^{10} μm^{-3})	SS (10^{-3} μm)	$\bar{C}_{\text{expt}}$ (10^{21} cm^{-3})	$\bar{C}_{\text{expt}}$ Equation (1)	$\bar{C}'$ Equation (2)
300	0.48	0.4	2			4	0.1	0.0863
350	0.4	0.2	3			3.7	0.0925	0.0863
400	0.37	0.1	1.5			3.37	0.0842	0.08
420	0.37	0.1	0.6			3.6	0.09	0.075
440	0.37	0.19	1.3			3.07	0.0767	0.074
460	0.32	0.21	1.3			2.62	0.0655	0.065
480	0.285	0.31	1.25			2.17	0.0543	0.0565
500	0.25	0.31	1	1.3	3.5	1.75	0.0437	0.046
520	0.152	0.31	1.2	0.25	0.5	1.15	0.0287	0.03
540	0.105	0.4	1	0.17	0.5	0.7	0.0175	0.0163
560	0.06	0.42	1	0.18	0.5	0.396	0.0099	0.01139
580	0.04	0.45	0.9	0.13	20	0.365	0.0091	0.00725
600	0.03	0.4	0.85	0.13	20	0.18	0.0045	0.006
640	0.019	0.4	0.76	0.9	26	0.01	0.0025	0.00387

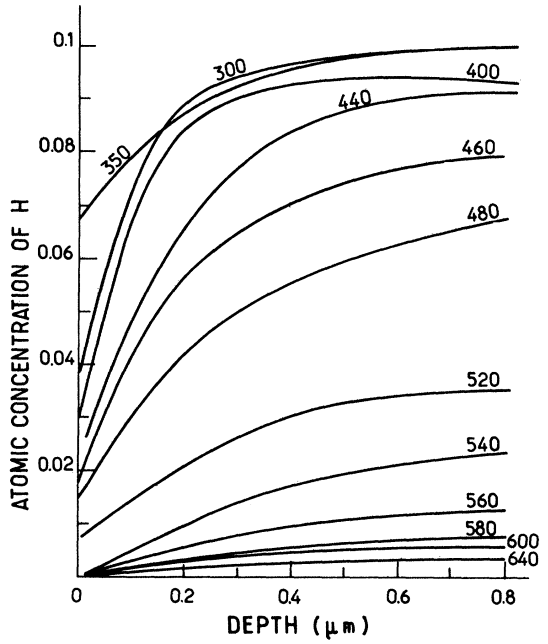

FIG. 9. Variation of the hydrogen atomic concentration $C_{expt}(x)$ versus depth x [from Eq. (1)] deduced from nuclear reaction measurement for the samples of series 3. Each of them annealed 30 min at a given temperature.

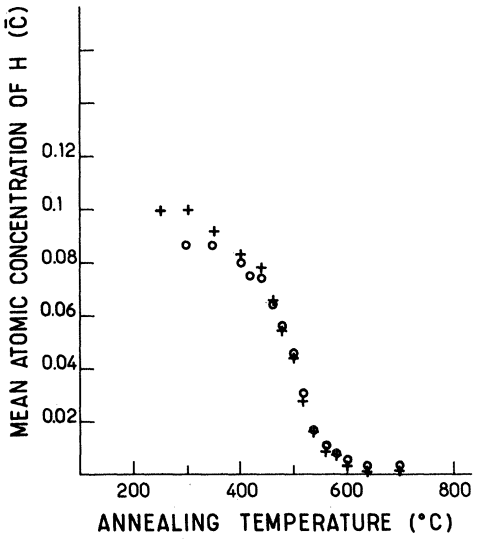

FIG. 10. Variation of the mean hydrogen atomic concentration $\bar{C}$ versus annealing temperature for samples of series 3 [each o (or +) describes one sample after an anneal of 30 min at a given temperature] using the integration of two different profiles: o, constant profile given by Eq. (2); +, profile given by Eq. (1).

where e is the thickness of the sample. Values of $\bar{C}_{expt}$ deduced from Eqs. (1) and (2) are shown in Table II and plotted versus annealing temperature in Fig. 10. We can see in this figure that $\bar{C}_{expt}$ values are weakly dependent of the choice of the profile.

Figure 10 shows that the total atomic concentration $\bar{C}_{expt}$ in the sample decreases monotonically with increasing annealing temperature for $640 \geq T \geq 350$ °C. The first decrease of $\bar{C}_{expt}$ is observed at 350 °C. For T greater than 640 °C, $\bar{C}_{expt}$ stays constant even when the crystallization has taken place. For T lower than 350 °C, $\bar{C}_{expt}$ has a maximum constant value. Figure 10 shows that most of the hydrogen leaves the sample for annealing temperature below 500 °C (beginning at the second stage seen on conductivity). This departure of H below 500 °C will be interpreted as a diffusion process with an activation energy of 1.5 eV (this will be discussed in the following section).

E. Correlation

The different annealing stages shown by the different techniques are compared in Fig. 11, which summarizes our experimental results presented above. In this figure, nuclear reaction measurements $[\bar{C}_{expt}(T)]$ show a departure of hydrogen at 350 °C, whereas ir measurements $[C_{SiH}(T)]$ show that hydrogen departure occurs at 410 °C. We cannot conclude that these two temperatures are clearly distinct by considering these results alone, but conductivity measurements (the conductivity is measured at 60 °C, so it is sensitive to the hydrogen in the Si–H configuration) which show an annealing stage occurring at 450 °C confirm the ir results. In this case we cannot confuse this stage in σ (450 °C) with that seen in nuclear reaction measurements (350 °C). Otherwise, nuclear reaction measurements show a total hydrogen concentration of 0.1 before annealing, whereas we obtain a hydrogen concentration (Si–H configuration) of 0.04 using ir measurement. Thus we conclude that there is 6% of hydrogen which is infrared inactive. This leads us to consider that hydrogen can occupy two kinds of sites in the amorphous network: The first one is in the Si–H configuration and will be called "tightly bound hydrogen" (TBH), which starts to move above 410 °C; the second one is not covalently bonded to silicon, is infrared inactive and will be called "weakly bound hydrogen" (WBH). It starts to move at 350 °C. We note that ir measurements do not give information about hydrogen evolution above 520 °C, while we observe an EPR signal at this temperature.

On the other hand, Fig. 10 shows that 80% of the hydrogen content leave the sample below 520 °C.

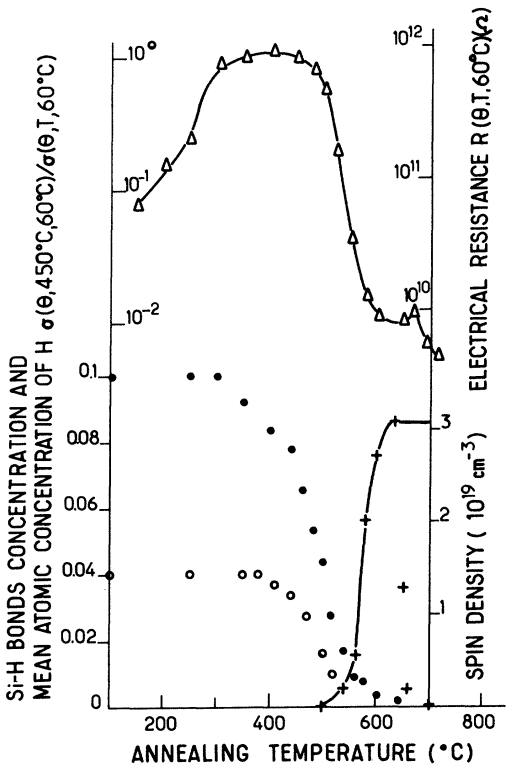

FIG. 11. Recapitulation of Figs. 1, 4, 8, and 10. △, variation of the electrical resistance $R(\theta, T, 60\,°C)$ and $\sigma(\theta, 450\,°C, 60\,°C)/\sigma(\theta, T, 60\,°C)$ versus annealing temperature on a silicon film of series 1. The solid line connects experimental points. ○, variation of the Si-H bond concentration $C_{SiH}(T)$ versus annealing temperature. +, variation of the mean spin density $C_{spin}(\theta, T, 20)$ versus annealing temperature (from Fig. 4). The solid line presents the theoretical model after Eq. (16) and Table VI. •, variation of the mean atomic concentration $\bar{C}_{expt}$ versus annealing temperature (from Fig. 10).

Above this temperature we observe the hydrogen departure by nuclear reaction, EPR, and conductivity measurements. From all these results it appears clearly that we have to consider three temperature intervals for the hydrogen evolution. For $300 < T \leq 410$ °C we observe the diffusion of the WBH out of the layer (nuclear measurement). For $410 < T < 520$ °C both diffusion of WBH and departure of a part of the TBH (nuclear reactions and ir measurements) take place. We assume that TBH makes the transition to WBH and then diffuses out of the layer. The inverse transition is considered to be possible. For $520 \leq T \leq 640$ °C we observe the diffusion of the WBH and the breaking of the Si–H bond (nuclear reaction and EPR measurements). All these considerations will be extensively studied elsewhere.[37] Here we will offer a phenomenological interpretation. We will attempt using nuclear reaction measurements to calculate a phenomenological diffusion coefficient for temperatures ranging from 350 °C to 500 °C as has been done by other authors.[13, 20, 22] Thus we will interpret the hydrogen evolution in this temperature range as due to a diffusion process (this will be justified later). We will show that hydrogen evolution above 500 °C is associated with a first-order process with an activation energy of 3.4 eV.

IV. DISCUSSION

A. Departure of hydrogen for $300 < T \leq 500$ °C

The phenomenological diffusion coefficient which will allow us to interpret our experimental results is due to the WBH and TBH, which move for $T \leq 500$ °C. Let us call $C(x,t)$ the total concentration of hydrogen atoms in the sample at a distance x from the external surface at a time t. It can be written

$$C(x,t) = C_1(x,t) + C_2(x,t), \tag{5}$$

where $C_1(x,t)$ is the concentration of the hydrogen which diffuses for $T \leq 500$ °C; it corresponds to the WBH and C_{SiH} (concentration of SiH) moving for $T \leq 500$ °C. $C_2(x,t)$ is the concentration of SiH which leaves the sample above 500 °C. The initial concentration of C_2 is equal to

$$C_{20} = 0.02 \simeq C_{SiH}\,(520\ °C),$$

so the initial concentration of C_1 is

$$C_{10} = 0.08.$$

For annealings below 520 °C, $C_2(x,t)$ is constant,

$$C_2(x,t) = C_{20}. \tag{6}$$

We assume that $C_1(x,t)$ will vary according to the equation

$$\frac{\partial C_1(x,t)}{\partial t} = D\,\frac{\partial^2 C_1(x,t)}{\partial x^2}, \tag{7}$$

where D is the effective diffusion coefficient of hydrogen. At the beginning of the annealing, the sample is assumed to be homogeneous: $C_1(x,t) = C_{10}$ at $t = 0$ and $0 < x < e$. On the other hand, the boundary conditions corresponding to exodiffusion are

$$\left.\begin{aligned} &C_1(x,t) = 0 \quad \text{for } x = 0 \\ &\left.\frac{\partial C_1}{\partial x}\right|_{x=e} = 0 \end{aligned}\right\} \text{for } t > 0. \tag{8}$$

The first equation describes the evolution of WBH atoms from the external surface ($x = 0$). The second one implies that there is no hydrogen diffusion from the film to the substrate. One can

easily verify that the solution of Eq. (7) satisfying these initial and boundary conditions is

$$C_1(x,t)=C_{10}\sum_{m=0}^{\infty}\frac{4}{\pi(2m+1)}\sin(2m+1)\frac{\pi x}{2e}\times\exp\left(-D\frac{(2m+1)^2\pi^2 t}{4e^2}\right). \quad (9)$$

The theoretical expression of the concentration profile $C(x,\theta,T)$ after an isothermal anneal at a temperature T and a time $t=\theta$ is obtained from Eqs. (5), (6), and (9)

$$C(x,\theta,T)=C_{10}\sum_{m=0}^{\infty}\frac{4}{\pi(2m+1)}\sin(2m+1)\frac{\pi x}{2e}\times\exp\left(-D(T)\frac{(2m+1)^2\pi^2}{4e^2}\theta\right)+C_{20}, \quad (10)$$

with $D(T)=D_0e^{-(E_D/k_BT)}$ where D_0 and E_D are independent of T.

In order to test the validity of our model, theoretical profiles $C(x,\theta,T)$ will be compared with experimental ones $C_{expt}(x,T)$ (Fig. 9), obtained from nuclear profiling measurements. Both are plotted in Figs. 12 and 13 for several temperatures. This comparison provides for each temperature a value of the effective diffusion coefficient D for hydrogen. In Table III we present D values for various temperatures, and the corresponding theoretical profiles $C(x,\theta,T)$ are plotted in Fig. 14.

All these profiles present a nonzero surface concentration $C(x=0,\theta,T)=C_{20}$ because the simple model used assumes that the TBH does not diffuse even at the neighborhood of the external surface, and the surface concentration of the diffusing hydrogen is zero (exodiffusion). It is important to see if this general feature of theoretical profiles is confirmed by experimental ones. As a matter of fact, Figs. 12 and 13 show that below 520 °C experimental and theoretical profiles are in correct agreement, and above this temperature, the fit is no longer possible because Eq. (6) is no longer valid since the TBH atoms [whose concentration is $C_2(x,t)$] start to move. (So the analysis of the nuclear profiles allows us to confirm the existence of a temperature of departure of a part of the THB above 500 °C.) On the other hand, Figs. 12 and 13 show some differences between theoretical and experimental profiles which are probably due to the choice we made for the function $C_{expt}(x)$ [Eq. (1)].

We shall now use this model [Eq. (10)] to obtain a simplified expression of D. The theoretical mean atomic concentration of H is

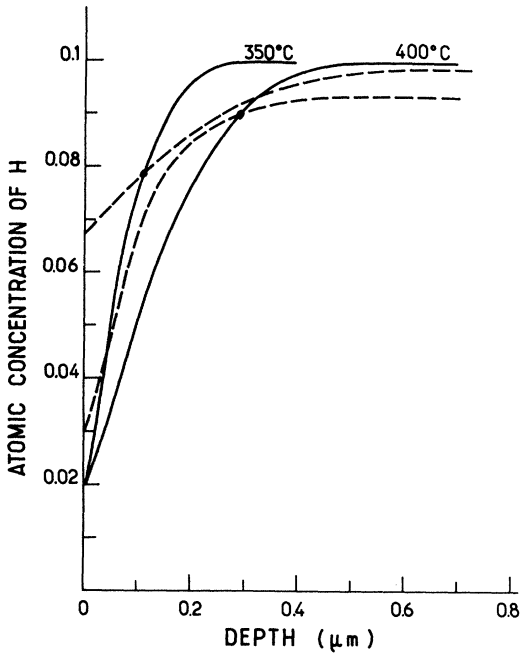

FIG. 12. Variation of the hydrogen atomic concentration versus depth obtained from ———, Eq. (10) (diffusion theory) and ---, Eq. (1) (experimental results) for various annealing temperatures.

$$\bar{C}(\theta,T)=\frac{1}{e}\int_0^e C(x,\theta,T)dx. \quad (11)$$

Substituting Eq. (10) in (11) and after integration, one obtains

$$\bar{C}(\theta,T)=\frac{8C_{10}}{\pi^2}\exp\left(-D(T)\frac{\pi^2\theta}{4e^2}\right)+C_{20}. \quad (12)$$

If we neglect C_{20} ($\simeq 0.02$) compared to C_{10} ($\simeq 0.08$), then $C_{10}\simeq C_0$, which is the initial total concentration of H. If we assume that $D\pi^2\theta/4e^2$ is such that all terms for $m>0$ in the series [Eq. (10)] are very small compared to the first one ($m=0$), then

$$\bar{C}(\theta,T)\simeq\frac{8C_0}{\pi^2}\exp\left(-D(T)\frac{\pi^2\theta}{4e^2}\right). \quad (13)$$

In order to get D we will compare the $\bar{C}(\theta,T)$ values obtained from Eq. (13) with the mean atomic concentration of hydrogen $\bar{C}_{expt}$ deduced from Eq. (1), presented in Fig. 10. Equation (13) gives

$$D=\frac{4e^2}{\pi^2\theta}\log_{10}\left(\frac{8C_0}{\bar{C}(\theta,T)\pi^2}\right). \quad (14)$$

Values of D deduced from Eq. (14) and Table II are presented in Table IV.

In Fig. 15 we have plotted $\log_{10}D$ vs $1000/T$. Values of D deduced from simplified equation (14) seem to be in good agreement with D values deduced

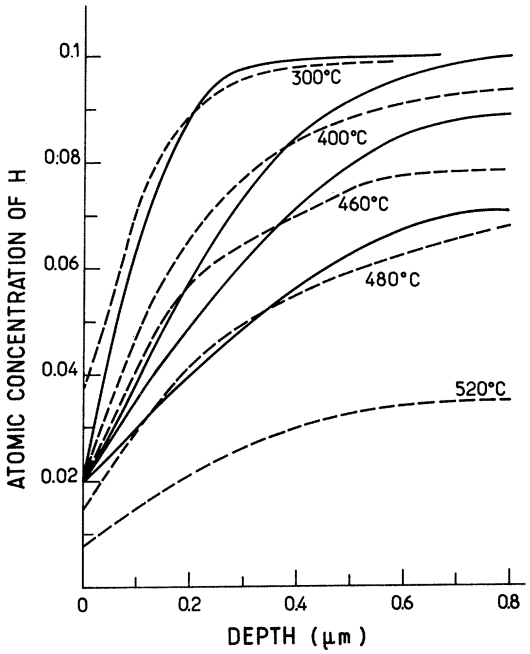

FIG. 13. Variation of the hydrogen atomic concentration versus depth obtained from ——— Eq. (10) (diffusion theory) and --- Eq. (1) (experimental results) for various annealing temperatures.

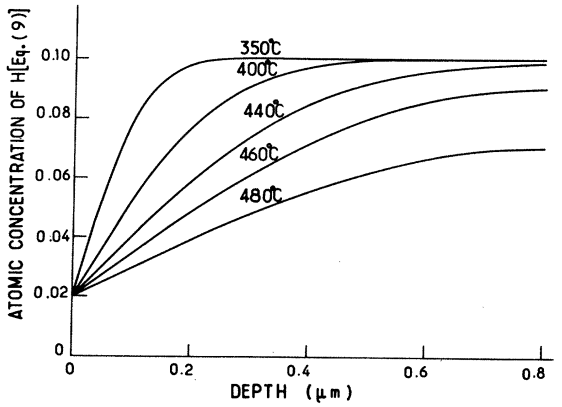

FIG. 14. Variation of the hydrogen atomic concentration $C(x, \theta, T)$ versus depth x, deduced from diffusion theory, using values of D given in Table III for various temperatures.

from the complete calculation (Table III). This provides an activation energy $E_D = 1.5$ eV and $D_0 = 4.7 \times 10^{-3}$ cm^2/s.

B. ir results

If we try to interpret our experimental results for temperatures ranging from 420 to 500 °C as being due to a first-order process, we can write $C_{SiH}(T,t) = [C_{SiH}(0) - C_{20}]e^{-K_3 t} + C_{20}$, where $K_3(T) = K_{30} e^{-E_3/k_B T}$ and $C_{SiH}(T,t)$ and $C_{SiH}(0)$ are, respectively, the concentrations of the Si–H bonds at a time t and before annealing. The comparison of the solution with experimental results gives a value of $K_3(T)$ for each temperature. The values of K_3 are given in Table V and plotted in Fig. 16. We obtain an activation energy $E_3 = 1.4 \pm 0.3$ eV. This value is nearly equal to the activation energy of the diffusion coefficient for the hydrogen evolution between 350 and 500 °C.

C. Hydrogen departure for $T > 500$ °C

Experimental results allow us to provide a quantitative description of the departure of the TBH atoms which move above 500 °C. The simplest model assumes that H atoms diffuse from a TB site to the nearest neighbor TB, assuming it is free. We have evaluated the initial concentration of filled TB centers to be 0.04. This corresponds to a distance of $\simeq 4$ atomic distances, so that such a diffusion process appears improbable. We assume that in order to leave the sample, TBH atoms must make a transition from a TB center to a WB one. Then they can diffuse out of the sample with a diffusion coefficient D previously determined. If the inverse process of capture of a WBH atom by a TB center can be neglected, the total process is controlled by a first-order law,

$$\frac{d\bar{C}_2}{dt} = -K_2(T)\bar{C}_2, \tag{15}$$

where $K_2(T)$ is a thermally activated characteristic frequency of the transition from a TB center to a WB one ($K_2 = K_{20} e^{-E_2/k_B T}$). The TBH atoms leave

TABLE III. Values of the diffusion coefficient D obtained from comparison of experimental profiles [Eq. (1)] with theoretical ones [Eq. (10)].

T (°C)	350	400	440	460	480
$1000/T$ (K^{-1})	1.605	1.485	1.402	1.364	1.328
$\frac{D\Pi^2}{4e^2}$ (s^{-1})	8.33×10^{-6}	3.83×10^{-5}	1×10^{-4}	1.96×10^{-4}	3.9×10^{-4}
D (cm^{2}s^{-1})	2.13×10^{-14}	9.8×10^{-14}	2.55×10^{-13}	5.01×10^{-13}	9.94×10^{-13}

TABLE IV. Values of the diffusion coefficient D obtained from the simplified equation (14).

T (°C)	440	460	480	500	520	300
$1000/T$ (K^{-1})	1.4	1.36	1.32	1.29	1.26	1.74
$\bar{C}_{expt}$	0.0767	0.0655	0.0543	0.0437	0.0287	0.1
D ($cm^2 s^{-1}$)	8×10^{-14}	4.44×10^{-13}	5.77×10^{-13}	8.9×10^{-13}	1.5×10^{-12}	

their sites independently of each other. This implies that if the TBH atoms are homogeneously distributed in the sample at $t=0$, this homogeneity stays at later times. We will interpret here our results using Eq. (15). In these conditions the solution can be written

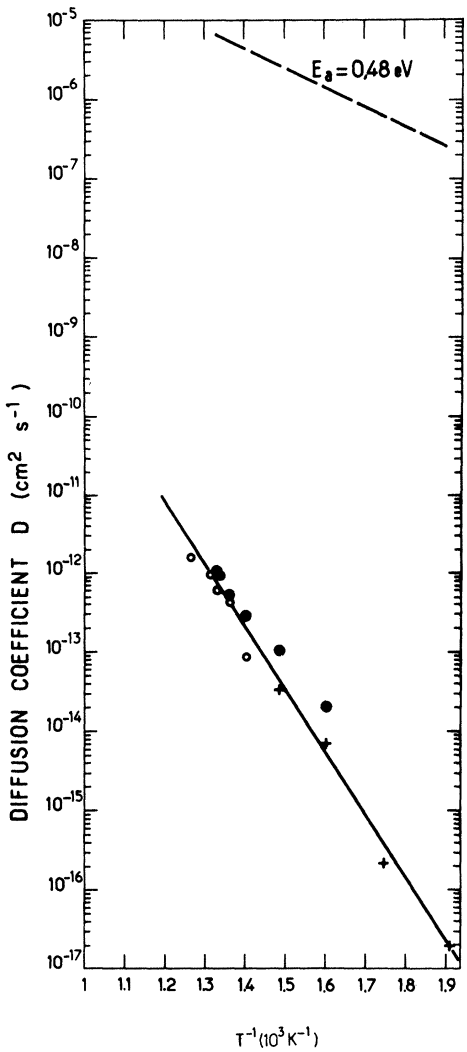

FIG. 15. Variation of $\log_{10} D$ vs $1000/T$ for ●, our results on samples of the 3 series (Table III); ○, results on samples of the 3 series (Table IV); +, Carlson results (Ref. 22); ⊕, Dieumegard results (Ref. 20); ----, Interstitial diffusion of hydrogen in crystalline silicon after Ref. 46.

$$C_2(t,T)=C_{20}\exp[-K_2(T)t]\,. \tag{16}$$

If we assume that the spin concentration is proportional to the concentration of TBH atoms which have leaved the sample,

$$C_{spin}(t,T)=\alpha[C_{20}-\bar{C}_2(t,T)]\,. \tag{17}$$

α is a dimensionless coefficient ($\alpha<1$) which takes into account a possible rearrangement of binding after the rupture of the Si-H complexes. αC_{20} is interpreted as the maximum spin density when the total TBH content is zero; after an extensive isothermal anneal $\alpha C_{20}=C_{spin}(\infty)=3\times10^{19}$ cm^{-3},

$$C_{spin}(t,T)=C_{spin}(\infty)\{1-\exp[-K_2(T)t]\}\,. \tag{18}$$

We shall now present the comparison of this model with EPR experimental results (Fig. 11). This comparison provides values of K_2 for each annealing temperature T. Experimental values of $C_{spin}(\theta, T, 20\,°C)$ and the corresponding values of K_2 deduced from Eq. (18) are presented in Table VI and Fig. 16, in which we have plotted the variations of $\log_{10} K_2$ vs $1000/T$. This provides $K_{20}=2.3\times10^{16}$ s^{-1} and $E_2=3.4\pm0.2$ eV. The fact that E_2 is equal to the Si–H bond energy[36] is direct evidence that the appearance of the EPR signal is due to the breaking of the Si–H bond.

We would now like to interpret the isothermal annealing of the conductivity (Fig. 3) using the above model [Eq. (18)]. For this we must correlate EPR and conductivity measurements.

D. Relation between spin concentration and conductivity

Figure 11 allows us to deduce that for annealing temperature above 500 °C, the mean spin concentration and mean conductivity increase (departure of TBH atoms) when the mean atomic concentration of hydrogen decreases. On the other hand, Fig. 9 shows that at a given temperature

TABLE V. Values of K_3 obtained from ir measurements.

T (°C)	410	440	470
$1000/T$ (K^{-1})	1.464	1.4	1.345
K_3 (s^{-1})	9×10^{-5}	2×10^{-4}	5.2×10^{-4}

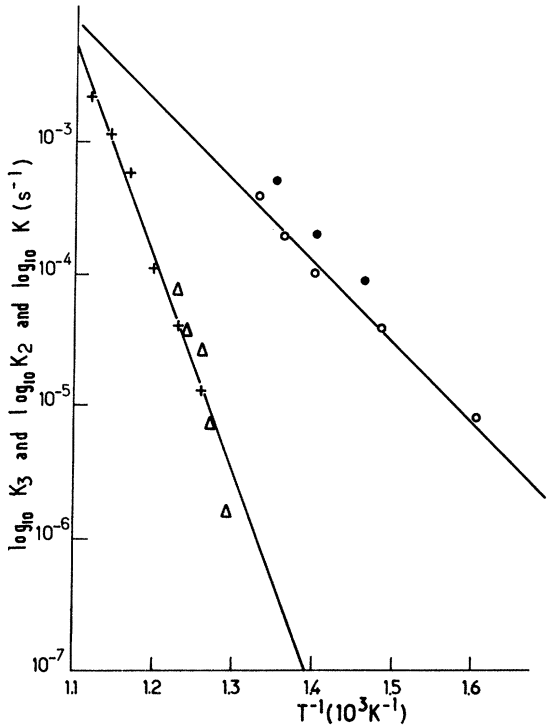

FIG. 16. +, Variation of $\log_{10} K_2$ vs $1000/T$ deduced from EPR measurements; △, same variation deduced from the correlation of σ measurements with those of EPR; ○, variation of $\log_{10}$ ($K = \pi^2 D/4e^2$) vs $1000/T$; ●, variation of $\log_{10} K_3$ vs $1000/T$ deduced from ir measurements.

$C_{\text{expt}}(x=0) \ll C_{\text{expt}}(x=e)$. So one can simply describe the behavior of the sample assuming the existence of a surface layer having a conductivity σ_α, equal to that of the amorphous evaporated film and a spin concentration $C_{\text{spin}}(\infty)$, as follows:

$$\sigma(\theta, T, 60\,^\circ\text{C}) = \sigma_\alpha \frac{e_\sigma^{\text{eff}}(\theta, T)}{e} \tag{19}$$

and

$$C_{\text{spin}}(\theta, T, 20\,^\circ\text{C}) = C_{\text{spin}}(\infty) \frac{e_{\text{EPR}}^{\text{eff}}(\theta, T)}{e'}, \tag{20}$$

where e_σ^{eff} and $e_{\text{EPR}}^{\text{eff}}$ are the effective thicknesses of the surface dehydrogenated layer (SDL) and e and e' are, respectively, the total thicknesses for the 1 and 3 series. Figures 1 and 11 show that the values of $C_{\text{spin}}(\theta, T, 20\,^\circ\text{C})$ and of $\sigma(\theta, T, 60\,^\circ\text{C})$ corresponding to $T = 520\,^\circ\text{C}$ are, respectively, 2.08×10^{18} cm^{-3} and 1.8×10^{-7} $(\Omega\,\text{cm})^{-1}$. Equations (19) and (20) provide, respectively, $e_\sigma^{\text{eff}}(T = 520\,^\circ\text{C}) = 320$ Å and $e_{\text{EPR}}^{\text{eff}}(T = 520\,^\circ\text{C}) = 550$ Å. These values of the effective thickness show that the very simple SDL model gives correct results. This leads us to correlate

TABLE VI. Values of $C_{\text{spin}}(\theta, T, 20\,^\circ\text{C})$ obtained from EPR measurements, K_2 obtained from comparison of EPR experimental results [$C_{\text{spin}}(\theta, T, 20\,^\circ\text{C})$] with Eq. (18), and K_2' obtained from comparison of the correlation of conductivity and EPR measurements with Eq. (18).

T (°C)	500	510	520	530	540	560	580	600	620	640
$C_{\text{spin}}(\theta, T, 20)$ (10^{19} cm^{-3})	0		0.07		0.21	0.56	1.95	2.62	2.94	3
$1000/T$ (K^{-1})	1.29	1.277	1.26	1.245	1.23	1.20	1.17	1.145	1.12	1.095
K_2 (s^{-1})			1.3×10^{-5}		4×10^{-5}	1.1×10^{-4}	5.8×10^{-4}	1.15×10^{-3}	2.2×10^{-3}	
K_2' (s^{-1})	1.48×10^{-6}	7.14×10^{-6}	2.66×10^{-5}	3.7×10^{-5}	7.6×10^{-5}					

the experimental results (Fig. 11) represented by the variations of $\sigma(\theta, 450\,^{\circ}\mathrm{C}, 60\,^{\circ}\mathrm{C})/\sigma(\theta, T, 60\,^{\circ}\mathrm{C})$ and the spin concentration $C_{spin}(\theta, T, 20\,^{\circ}\mathrm{C})$ versus annealing temperature. We note that $\sigma(\theta, 450\,^{\circ}\mathrm{C}, 60^{\circ}\mathrm{C})$ corresponds to the maximum value of the electrical resistance just at the beginning of the second annealing stage described in Sec. III B. The measured value of $\sigma(\theta, 450\,^{\circ}\mathrm{C}, 60\,^{\circ}\mathrm{C})$ is very close to that of $\sigma(450\,^{\circ}\mathrm{C}, 60\,^{\circ}\mathrm{C})$, which is defined in Sec. II B 1. This correlation is presented in Fig. 17, where $\log_{10}\sigma(\theta, 450\,^{\circ}\mathrm{C}, 60\,^{\circ}\mathrm{C})/\sigma(\theta, T, 60\,^{\circ}\mathrm{C})$ is plotted versus $\log_{10}C_{spin}(\theta, T, 20\,^{\circ}\mathrm{C})$; here the annealing temperature is a hidden parameter. The lower and upper limits for the error bars (Fig. 17) are, respectively, obtained by using the isochronal results for σ (Fig. 11) and the values of the electrical resistance after an isothermal annealing (Fig. 3) at a temperature T during a time of 30 min. If we assume that $e_{\sigma}^{eff}(T) = e_{EPR}^{eff}(T)$ in the SDL model, Eqs. (19) and (20) show that it is represented in Fig. 17 by a straight line with a slope equal to -1, which gives the best fit for the correlation curve. We can see that the data agree with the SDL model except near the maximum value of the spin density.

We can now deduce the variations of the spin density $C_{spin}(t, T, 20\,^{\circ}\mathrm{C})$ after an isothermal annealing at temperature T for a time t, from the variations of $\sigma(450\,^{\circ}\mathrm{C}, 60\,^{\circ}\mathrm{C})/\sigma(t, T, 60\,^{\circ}\mathrm{C})$ versus annealing time t (Fig. 3) and from the results presented by the experimental correlation curve in Fig. 17. These variations of $C_{spin}(t, T, 20\,^{\circ}\mathrm{C})$ vs t are presented in Fig. 18.

If the above correlation is valid, the variations of $C_{spin}(t, T, 60\,^{\circ}\mathrm{C})$ versus t must satisfy Eq. (18). Figure 19 shows the calculation of $\ln\{C_{spin}(\infty)/[C_{spin}(\infty) - C_{spin}(t, T, 20\,^{\circ}\mathrm{C})]\}$ versus annealing time for various isothermal annealing temperatures. We observe a linear variation $\ln\{C_{spin}(\infty)/[C_{spin}(\infty) - C_{spin}(t, T, 20\,^{\circ}\mathrm{C})]\} = K_2'(T)t$ so that Eq. (18) is satisfied. Values of K_2' are given in table VI. The variation of $\log_{10}K_2'$ vs $1000/T$ is presented in Fig. 16, which shows good agreement with the $K_2(T)$ values deduced from EPR measurements. For K_2 we obtain $K_{20} = 2.3 \times 10^{16}\ \mathrm{s}^{-1}$ and $E_2 = 3.4 \pm 0.2$ eV. This activation energy, which is associated with the departure of TBH atoms, can be identified with the binding energy of Si–H which is 3.4 eV.

The good agreement of values of K_2 deduced from direct EPR experimental results with K_2' values deduced from conductivity measurement (Fig. 3) using the correlation between conductivity and EPR measurements (Fig. 17) allows to conclude to the validity of the SDL model. We shall show that conductivity measurements (Fig. 2) can be interpreted in this way.

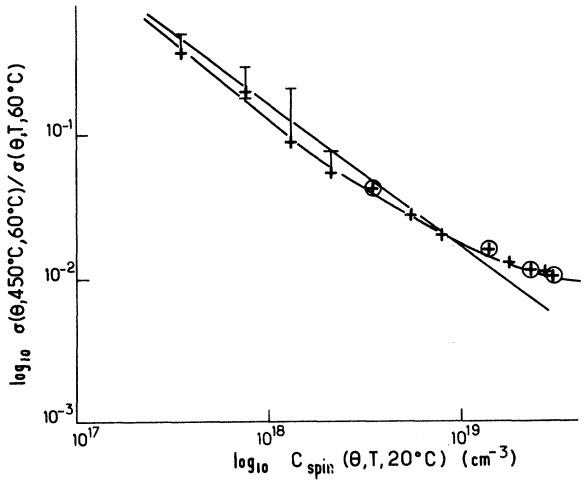

FIG. 17. Variation of $\log_{10}\sigma(\theta, 450\,^{\circ}\mathrm{C}, 60\,^{\circ}\mathrm{C})/\sigma(\theta, T, 60\,^{\circ}\mathrm{C})$ vs $\log_{10}C_{spin}(\theta, T, 20\,^{\circ}\mathrm{C})$ deduced from Fig. 11: ⊕, experimental results; +, the solid curve is obtained by correlation of the two solid curves (on conductivity and EPR measurement) of Fig. 11. The straight line has a slope equal to -1.

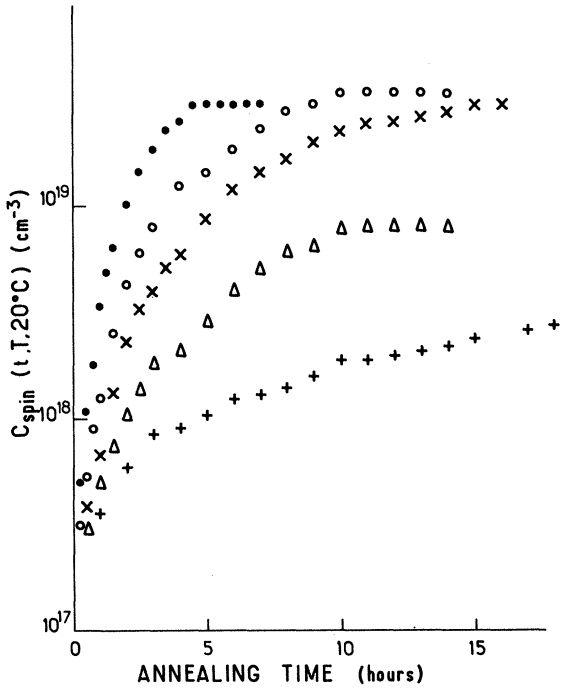

FIG. 18. Variation of the mean spin density $C_{spin}(t, T, 20\,^{\circ}\mathrm{C})$ versus annealing time during isothermal run deduced from Figs. 3 and 17: +, 500 °C; △, 510 °C; ×, 520 °C; ○, 530 °C; ●, 540 °C.

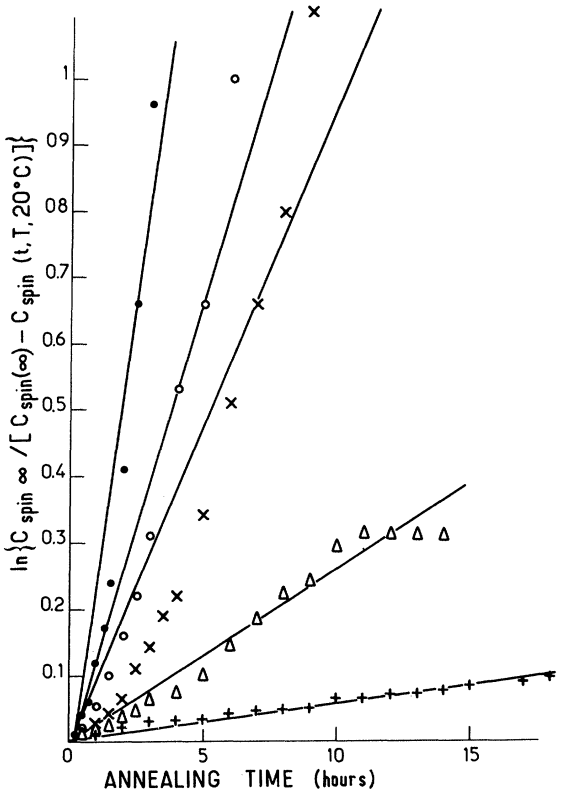

FIG. 19. Variation of ln $\{C_{spin}(\infty)/[C_{spin}(\infty) - C_{spin}(t, T, 20\,°C)]\}$ versus annealing time deduced from Fig. 18: +, 500 °C: △, 510 °C; ×, 520 °C; ○, 530 °C; ●, 540 °C.

E. Detailed discussion of conductivity measurements

We can now attempt to interpret the behavior of $\log_{10}\sigma$ vs $1000/T$ after each isochronal annealing during the second stage (Fig. 2, curves $1a$–$2b$). First we shall show that the conduction is not due to donor (or acceptor) centers produced by departure of hydrogen. We assume that the material is homogeneous at the beginning and throughout the second stage. If we assume that the departure of hydrogen leaves electric centers acting as donors (or acceptors), we can write the extrinsic carrier concentration as[38]

$$n_{ext} = 2\left[\left(\frac{mk_BT}{h^2}2\pi\right)^{3/2} N_D\right]^{1/2} \exp\left(-\frac{E_0}{2k_BT}\right), \quad (21)$$

where N_D and E_0 are, respectively, the donor (acceptor) concentration and its energy, referred to the bottom (top) of the conduction (valence) band. m and h are, respectively, the electron mass and the Planck constant. The mobility carrier is about 1–10 $cm^2 V^{-1} s^{-1}$.[39] After an isochronal run at 500 °C our experimental results on series 1 give $\sigma = \sigma_0 e^{-E/k_BT}$ with $\sigma_0 = 6 \times 10^{-4}$ $(\Omega\,cm)^{-1}$ and $E = 0.13$ eV (in the room-temperature range). Comparison with Eq. (21) gives $N_D = 10^2$ cm^{-3}. The aberrant value of N_D shows the inadequacy of such a model. This model is inadequate in the whole temperature range (400 °C–640 °C).

We will also show that conduction is not due to surface effects such as band bending.[40] The equalization of the chemical potentials at the amorphous-substrate interface implies the existence of a potential barrier (whose thickness is related to the screen length in the material). In the hydrogenless evaporated amorphous silicon, the room-temperature carrier concentration is large, and this band-bending effect should not appear, but in the case of hydrogenated amorphous silicon, Solomon *et al.*[40] have shown that because of the very low room-temperature carrier concentration, this surface effect is important. These authors show that the electrical conductivity of the material can be written $\sigma_{app} = \sigma_v + (\delta/e)\sigma_s$ where σ_{app} is the apparent conductivity of the sample, σ_v is the bulk conductivity, and σ_s is the surface conductivity. $\sigma_v = \sigma_0 e^{-E/k_BT}$ and $\sigma_s = \sigma_0 e^{-(E-qV_s)/k_BT}$, both thermally activated, q is the electronic change, V_s the surface potential, e the thickness of the sample, and δ its effective thickness. Using the above conduction model, Solomon *et al.* interpret conductivity measurements of hydrogenated amorphous silicon films performed by Stabler and Wronsky[41] at room temperature. These authors show that their samples have two completely different sets of properties after annealing above 150 °C: state A with a conductivity $\sigma_A = \sigma_{0A} \exp(-E_A/k_BT)$ with $\sigma_{0A} = 4 \times 10^3$ $(\Omega\,cm)^{-1}$ and $E_A = 0.5$ eV, or after intense illumination, state B with a conductivity $\sigma_B = \sigma_{0B} \exp(-E_B/k_BT)$ with $\sigma_{0B} = 10^5$ $(\Omega\,cm)^{-1}$ and $E_B = 0.87$ eV. The transition between the two states is reversible. Solomon *et al.*[40] interpret the state B as being very close to the flat band state ($\sigma_{app} \neq \sigma_v$) and state A as a state characterized by band bending. In this state, the phenomenon is controlled by a surface conduction

$$\sigma_{app} \neq (\delta/e)\,\sigma_s = (\delta/e)\,\sigma_0 \exp\left(-\frac{E - qV_s}{k_BT}\right).$$

Solomon *et al.* obtained from these results $\delta/e = \sigma_{0A}/\sigma_{0B} = 4 \times 10^{-2}$ and deduced a density of state in the gap $g \simeq 10^{16}$ $cm^{-3}\,eV^{-1}$. The application of the above-mentioned conduction model[40] to our samples of series 1 leads us to identify state A (Ref. 41) with the state represented by curve $1a$ in Fig. 2 (at room temperature), σ having been measured after an annealing of 30 min at 400°C. We get $\sigma_{A'} = \sigma_{0A'} \exp(-E_{A'}/k_BT)$ with $\sigma_{0A'} = 7.4 \times 10^{-6}$ $(\Omega\,cm)^{-1}$ and $E_{A'} = 0.16$ eV, giving $\sigma_{0A'} \neq (\delta/e)\sigma_0$. If we assume an intrinsic conduction mechanism at room temperature in the bulk of our sample,

the corresponding conductivity is provided by the extrapolation (curve 1*b*, Fig. 2) at room temperture of the intrinsic regime observed at high temperature (curve 1, Fig. 2). This gives us a state we will call B' with a conductivity $\sigma_{B'} = \sigma_{0B'} \exp(-E_{B'}/k_B T)$, where $\sigma_{0B'} = 2 \times 10^5$ $(\Omega\,\mathrm{cm})^{-1}$ and $E_{B'} = 0.85$ eV. This conductivity is very close to that of state B measured by Staebler and Wronsky.[42] From the model[40] $\sigma_{0B'} \simeq \sigma_0$. The above analysis gives for our results $\delta/e = \sigma_{0A'}/\sigma_{0B'} = 3.7 \times 10^{-11}$. This value of δ/e allows us to conclude that this model cannot be applied to our results.

We shall show that conduction can be interpreted using the SDL model. The above analysis leads to the idea that a hydrogenated amorphous silicon film after an isothermal anneal at 400°C is no longer in the physical initial state described by Solomon *et al.*,[40] Staebler *et al.*,[42] and Spear *et al.*[34] We think that in such a film, a very small quantity of hydrogen diffused out of the sample from a region very near the external surface, so that the electrical conductivity of this superficial zone is much greater than the conductivity inside the film where hydrogen atoms have not diffused. The thin superficial layer has an electrical conductivity close to that of evaporated amorphous silicon, and the conduction mechanism takes place in the surface layer. If the amorphous silicon film is again isothermally annealed at higher temperature ($\theta = 30$ min at $T = 450$°C, for instance), the effective thickness e^{eff} of the surface dehydrogenated layer participating in the conduction increases. This idea is confirmed as follows. Figure 2 shows that curves representing $\log_{10}\sigma$ vs $1000/T$ for temperatures ranging in the vicinity of room temperature, obtained after successive isochronal anneals of the sample, can be deduced from each other by translation. The behavior of $\log_{10}\sigma$ vs $1000/T$ is the same for all curves, but the effective thickness is different and increases with annealing temperature. An effective conductivity is measured and given by $\sigma_{\mathrm{eff}} = (e_\sigma^{\mathrm{eff}}/e)\,\sigma_\alpha = \sigma(\theta, T, 60°\mathrm{C})$ with $\sigma_\alpha = \sigma(\theta, 640°\mathrm{C}, 60°\mathrm{C}) = 3.4 \times 10^{-6}$ $(\Omega\,\mathrm{cm})^{-1}$ and $e = 6000$ Å. We note that for annealing temperatures between 400 and 500°C, conductivity measurements seem to show (in the SDL model) an effective thickness of $60 < e_\sigma^{\mathrm{eff}} < 100$ Å. This result is not inconsistent with EPR measurements, which are not sensitive enough in this range of temperature ($e_{\mathrm{EPR}}^{\mathrm{eff}} \simeq 0$ for $T < 500$°C), or with the nuclear profiling measurements whose depth resolution is 400 Å.

V. CONCLUSIONS

A. Diffusion coefficient

We have interpreted our experimental results for $T \leq 500$ °C as being due to a diffusion process. For comparison, we plot in Fig. 15 results from Carlson *et al.*,[22] Dieumegard *et al.*,[20] and Kaplan *et al.*[13]

One can see the very good agreement among all these series of results which have been obtained for amorphous materials prepared under various conditions with various hydrogen concentrations. These results give a diffusion coefficient D with an activation energy $E_D = 1.5$ eV for a variation of 5 orders of magnitude. This agreement implies a diffusion mechanism which is intrinsic to the amorphous material rather than a void controlled H diffusion, which would show scattered results for D due to the variation of the size and nature of voids. We have also presented in Fig. 15 values of D corresponding to the diffusion of the interstitial H in crystalline silicon.[42] This diffusion is thermally activated with $E_a = 0.48$ eV. The diffusion mechanism of H in amorphous and crystalline material appears completely different. The value of 1.5 eV for amorphous silicon implies a diffusion mechanism where the diffusing H atom interacts to a certain extent with the amorphous silicon random network. This cannot be an interstitial atomic diffusion.

B. Behavior of the Si-H bonds

We are mainly interested in the behavior of the Si–H bonds. On one hand, the ir measurements (which are sensitive to the Si–H bond) show that the hydrogen evolution occurs for temperatures ranging from 410 to 520 °C. This could be described by a first-order process with an activation energy of about 1.5 eV. On the other hand, EPR measurements show that the departure of hydrogen above 500 °C, which corresponds to the breaking of the Si–H bond, is controlled by a first-order process with an activation energy of 3.4 eV (Si–H bond energy). These results lead us to conclude that the TBH (Si–H configuration) has a completely different behavior when we consider either the first temperature interval ($410 \leq T < 520$ °C) or the second one ($520 \leq T \leq 640$ °C).

For annealing $T \leq 500$ °C, we observe a release of hydrogen from Si–H configuration (50% of the total TBH content). In this low-temperature range it is improbable that isolated Si–H bonds (which are very strong) release hydrogen. A long with Biegelson *et al.*[18,25] we think that a compensating energy-gain mechanism must be present. It should be due either to the bond reconstruction or to the possibility for two hydrogen atoms leaving in a coordinate way to form an H_2 molecule.[43] Such Si–H bonds should be very close to each other to facilitate the bond reconstruction, either in cluster forms in the amorphous network as

proposed by Mosseri *et al.*[44], or more generally in regions of Si–H high density. This bond reconstruction phenomenon should render the departure of H and its capture by a dangling-bond Si site faster than the diffusion of the WBH out of the layer. Then the limiting process should be the diffusion process. This could explain the fact that ir results provide an activation energy close to that of diffusion 1.5 eV for $T \leq 500\,^{\circ}C$.

For temperature higher than 500 °C, Si–H bonds release hydrogen with an activation energy equal to that of the Si–H bond energy (3.4 eV). We think that such Si–H bonds should be isolated in the amorphous network; then the predominant phenomenon is the breaking of the bond.

C. Possible configurations of H

The above exodiffusion model [Eqs. (6), (7), and (15)] which allowed us to interpret our experimental results involves two kinetic parameters D and K_2. We assume that the phenomenological coefficient D is close to D_1, the diffusion coefficient for the WBH. This will be shown later.[37] We shall now attempt to give for $D \simeq D_1$ and K_2 a configurational representation. We present in Fig. 20 possible configurations of hydrogen in the amorphous network. (i) A WBH atom in a three-center bond corresponding to the Si–H–Si configuration [position (c)], in which the hydrogen atom occupies a weakly bound position in the amorphous material. This model was proposed by Fisch *et al.*[45] One can think that the activation energy observed should correspond to the necessary energy for migration of H from an Si–H–Si site to the nearest-neighbor site of the same type. (ii) Another WBH configuration which should be possible is the H_2 molecule [position (e)] hopping from one interstitial position to another with an energy barrier of 1.5 eV. This picture given for the WBH would be in good agreement with the Fritzsche *et al.* observation[43] presented above. (iii) A TBH atom corresponding to the isolated Si–H configuration [position (d)]. We also present a plot of the variation of the total energy (or enthalpy) of the amorphous system versus the position of the hydrogen atom. Two cases are shown corresponding to the transition of a hydrogen atom from a TB site to a free neighboring WB one and the transition from a WB site to a free neighboring WB one. These transitions occur with activation energies respectively equal to 3.4 eV (Si–H bonding energy[36]) and 1.5 eV.

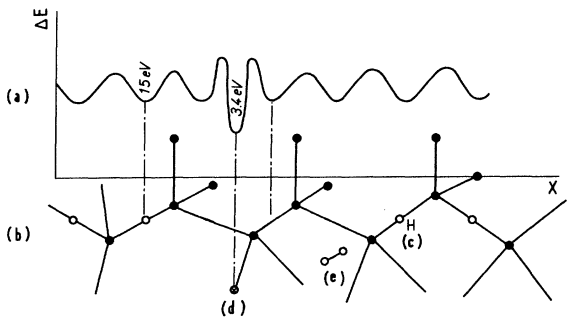

FIG. 20. (a) Variation of the total energy (or enthalpy) ΔE of the amorphous system versus the position x of the hydrogen atom corresponding to the transitions (from WBH to WBH and from TBH to WBH); (b) Two possible configurations: ○, WBH; Si–H–Si configuration [position (c)] and H_2 [position (e)]. ⊗, TBH; Si–H configuration [position (d)]. ●, Si.

D. Thermodynamical parameters

We want to calculate the thermodynamical parameters which are derived from the thermodynamical theory of diffusion and chemical reactions, i.e., from our parameters $D_1 \simeq D$ and K_2 (Ref. 46), D has been written $D = D_0 e^{-E_D/k_B T}$ when the transformation occurs at constant pressure and temperature:

$$D = \nu_D a^2 \exp(\Delta S_D/k_B) \exp(-\Delta H_D/k_B T), \qquad (22)$$

where $\Delta H_D \simeq E_D$ and ΔS_D are, respectively, the characteristic variation of enthalpy and entropy for diffusion and a is of the order of the interatomic distance; we will take $a = 3 \times 10^{-10}$ m. The WBH vibrational characteristic frequencies ν_D have not been observed; we will take $\nu_D = 10^{12}$ HZ. On the other hand, we can write $D_0 \simeq \nu_D a^2 \exp(\Delta S_D/k_B)$. Our experimental results give $D_0 = 4.7 \times 10^{-3}$ cm^2 s^{-1} and $E_D = 1.5$ eV. So we find $\Delta S_D = 1.65 k_B$.

In the same way, K_2 has been written $K_2 = K_{20} \exp(-E_2/k_B T)$; our experimental results give $K_{20} = 2.3 \times 10^{16}$ s^{-1} and $E_2 = 3.4$ eV. On the other hand, when the exodiffusion reaction occurs at constant pressure and temperature we can write

$$K_2 = \nu_2 \exp(+\Delta S_2/k_B) \exp(-\Delta H_2/k_B T), \qquad (23)$$

where ν_2 is a characteristic frequency of the vibrational mode of the Si–H bond and ΔH_2 and ΔS_2 are, respectively, the characteristic variations of enthalpy and entropy for the transition from a TB to a WB center. For the same reason as above we obtain $\Delta H_2 \simeq E_2 = 3.4$ eV. We take for ν_2 a value deduced from infrared absorption measurements (stretching modes $\nu_2 \simeq 9.5 \times 10^{12}$ or wagging modes $\nu_2 \simeq 3 \times 10^{12}$ Hz). The two vibrational modes should equally be responsible for the transition from a TB center to a WB one. We take, for example, $\nu_2 = 9.5 \times 10^{12}$ Hz; then we get $\Delta S_2 = 7.8 k_B$.

E. ir calibration

The calibration of the Si-H concentration obtained from ir has been criticized.[15] If we assume that, in fact, the calibration is not correct, then the correct hydrogen concentration is (10%) that given by nuclear reaction measurements, which are very accurate. In this hypothesis the whole hydrogen content is in the Si–H configuration with an initial concentration $C_0 = 0.1$. In these conditions, using nuclear reaction results, we admit that some of the hydrogen atoms in Si-H forms move at 350 °C. We have interpreted above (Sec. IV A) the hydrogen departure for $T \leq 500$ °C in terms of diffusion. We will now show that such a diffusion process is still able to render account of our experiments in the present hypothesis.

For $T \leq 500$ °C the transport process is necessarily a random hopping of a hydrogen atom from and Si–H bond to the nearest-neighbor Si site assuming it is free (i.e., it has a dangling bond). If we consider that for each time interval τ, a hydrogen atom at a distance x can jump a length $\pm a$ with probabilities, respectively, equal to $[1 - C(x \pm a)/C_M]$ (it corresponds to the probability for that the arrival site be free), where C_M is the maximum concentration of hydrogen. We can easily show that the hydrogen atomic transport is also described by the Fick diffusion equation considering $D = a^2/\tau$. Even when the whole hydrogen is in the Si–H configuration the diffusion coefficient D has an interpretation. We have simply assumed that the hydrogen that evolved leaves the sample without encountering any surface energy barrier. The activation energy ($\simeq 1.5$ eV) we find must be the necessary energy for the hydrogen atom to make the transition from an Si–H bond to the nearest-neighbor free site. The initial Si–H bond concentration (of 10%) would correspond to a distance of about two atomic distances, so such a transition is not impossible. The fact that we observe such a low activation energy (which is much lower than the Si–H bond energy) implies that a bond reconstruction mechanism must be present during the hydrogen jump.

For temperature higher than 500 °C our EPR results (and a part of σ results) show that the hydrogen departure occurs with the breaking of the Si–H bond (3.4 eV). These bonds should be more isolated in the amorphous network. We note that even in this hypothesis (Si–H configuration) Eqs. (6) and (7) as well as values of D (Tables III and IV) are still valid because 80% of the hydrogen content move for $T \leq 500$ °C and 20% of H are mobile for $T > 500$ °C.

On the other hand, we showed (Sec. IV B) that ir results ($410 \leq T \leq 520$ °C) should roughly be interpreted in terms of a first-order process. Such a process cannot be due to a release of hydrogen from Si–H bonds, for either a hydrogen molecule will be formed and it will diffused out of the layer, or we observe a departure of hydrogen atoms which diffuse interstitially and rapidly out of the sample. The first alternative leads us to consider the existence of a WBH which is inconsistent with our present hypothesis (which assumes that there is only TBH Si–H configuration in the layer). The second alternative implies that the limiting process is the first-order law but in this case, we can easily show that if the sample is homogeneous at $t = 0$, the nuclear profiles should stay flat at later time. This is inconsistent with the observed nuclear profiles. We note that a first-order process can be easily confused with a diffusion process for high values of $D\theta/e^2$. From this analysis it appears that ir results should not be associated to a first-order process, but rather to an H diffusion process. ir measurements are not able to provide an accurate description of diffusion phenomenon, for they give $\overline{C}$ instead of $C(x)$. For this reason, diffusion has been studied using only nuclear profiles.

F. Conclusion

The above results show that there are two possible interpretations: Either the Si-H concentration and the total hydrogen concentration are quite different, implying that a WBH must exist and diffuses (hypothesis 1), or the two concentrations are equal to 10%, implying that the only sites where the hydrogen can be bonded are the TB centers (Si–H bonds) (hypothesis 2).

In any case we have to admit the following.

(i) A hydrogen departure occurs at 350 °C, and for temperature ranging from 350 to 500 °C nearly 80% of the initial hydrogen content diffuse out of the sample with an activation energy of 1.5 eV in good agreement with previous results.[13,20,22,47] This departure is controlled by a diffusion mechanism. As a matter of fact, let us recall that in hypothesis 1 (C_{SiH} less than the total hydrogen concentration) we observe a diffusion of the WBH beginning at 350 °C and a part of the TBH which moves for $T \leq 500$ °C. It makes the transition to a WB site easily and then diffuses. This will be extensively studied later.[37] In the case of hypothesis 2 (C_{SiH} equal to the total H concentration) we observe a departure of a part the Si–H bonds which are very near to each other. A bound H can jump to the nearest-neighbor Si dangling bond with an energy of 1.5 eV. A

compensating energy-gain mechanism is present. Consequently we observe a simple diffusion process.

(ii) A hydrogen atom which leaves the sample, for $T > 500$ °C, must get over an energy barrier of 3.4 eV. This energy obtained from EPR measurements and the correlation between EPR and conductivity measurements can reasonably be identified with the Si–H bond energy. In the hypothesis 2 as well as hypothesis 1, we must admit in this temperature range that a hydrogen atom leaving its site must diffuse out of the sample. We will attempt to intepret our results EPR, conductivity, and nuclear reaction measurements for $T > 500$ °C assuming that when leaving the sample, the hydrogen atom breaks its bond (3.4 eV) and then diffuses out of the sample with a diffusion coefficient D (1.5 eV).[48]

Biegelsen *et al.*[18,25] observed hydrogen evolution for various kinds of amorphous Si-H films and particularly those containing only Si-H complexes. In this case they correlate the variation of the spin density ($\leq 10^{18}$ cm^{-3}) and the concentration of the hydrogen evolved. They observe a linear dependence of $\log_{10}(N_S$, the spin number) with the percentage of hydrogen evolved at low spin density $\leq 10^{18}$ cm^{-3} (for samples with only Si-H complexes). It was not possible in our case to make such a correlation for two reasons: (1) our EPR measurements have been performed with a sensitivity of spin density of about 10^{18} cm^{-3}; (2) this corresponds to a percentage of evolved hydrogen ranging from 0.8 to 1, which is too small a range. Such a hydrogen-evolved range corresponds to a saturation zone observed by Biegelsen *et al.*[18,25] for which they think that the differential spin increase is from 10^{-2} to 10^{-3} times the hydrogen evolution. In our case we have interpreted EPR results assuming a linearity between the spin density and the hydrogen evolved in the same range of percentage (0.8 to 1). This interpretation gives us an activation energy of 3.4 eV (Si–H bond energy).

ACKNOWLEDGMENTS

We thank J. Bourgoin, P. Baruch, and P. Mooney for stimulating discussions and A. Deneuville and B. Pajot for assistance with ir experiments.

[1]M. H. Brodsky, R. S. Title, K. Weiser, and G. D. Petit, Phys. Rev. B 1, 2632 (1970).
[2]P. J. Zanzucchi, C. R. Wronski, and D. E. Carlson, J. Appl. Phys. 48, 5227 (1977).
[3]A. K. Ghosh, T. McMahon, E. Rock, and H. Wiesmann, J. Appl. Phys. 50, 3407 (1979).
[4]P. A. Thomas, M. H. Brodsky, D. Kaplan, and D. Lepine, Phys. Rev. B 18, 3059 (1978).
[5]R. A. Street, J. C. Knights, and D. Biegelsen, Phys. Rev. B 18, 1880 (1978).
[6]W. Paul, A. J. Lewis, C. A. N. Connell, and J. D. Moustakis, Solid State Commun. 20, 969 (1976).
[7]W. E. Spear and P. G. Lecomber, Solid State Commun. 17, 1193 (1975).
[8]M. H. Brodsky, Thin Solid Films 40, L23 (1977).
[9]M. H. Brodsky, Thin Solid Films 50, 57 (1978).
[10]M. H. Brodsky, M. A. Frisch, and J. F. Ziegler, Appl. Phys. Lett. 30, 561 (1977).
[11]S. Oguz and M. A. Paesler, Phys. Rev. B 22, 6213 (1980).
[12]S. Oguz, R. W. Collins, M. A. Paesler, and W. Paul, J. Non-Cryst. Solids 35 & 36, 231 (1980).
[13]N. Sol, D. Kaplan, D. Dieumegard, and D. Dubreuil, J. Non-Cryst. Solids 35 & 36, 291 (1980).
[14]D. Kaplan, N. Sol, G. Velasco, and P. A. Thomas, Appl. Phys. Lett. 33, 440 (1978).
[15]C. J. Fang, K. J. Gruntz, L. Ley, M. Cardona, F. J. Demond, G. Müller, and S. Kalbitzer, J. Non-Cryst. Solids 35 & 36, 255 (1980).
[16]P. Thon, M. Odeh, M. J. K. Thomas, M. J. Tricker, J. Mc Gill, A. Wallace, and J. I. B. Wilson, J. Non-Cryst. Solids 35 & 36, 237 (1980).
[17]A. Deneuville, J. C. Bruyère, A. Mini, H. Kahil, R. Danielou, and E. Ligeon, J. Non-Cryst. Solids 35 & 36, 469 (1980).
[18]D. K. Biegelsen, R. A. Street, C. C. Tsai, and J. C. Knights, J. Non-Cryst. Solids 35 & 36, 285 (1980).
[19]K. Zellama, P. Germain, S. Squelard, J. Monge, and E. Ligeon, J. Non-Cryst. Solids 35 & 36, 225 (1980).
[20]D. Dieumegard and D. Dubreuil in *Proceedings of the Third International Conference on Sputtering, Nice, 1979,* edited by J. Fauvet (Société Francaise du Vide, Paris, 1979), p. 189.
[21]C. C. Tsai, H. Fritzsche, M. H. Tanielian, P. J. Gaczi, P. D. Persans, and M. A. Vesaghi, *Proceedings of the Seventh International Conference on Amorphous and Liquid Semiconductors, Edinburgh, 1977,* edited by W. E. Spear (University of Edinburgh, Edinburgh, 1977), p. 339.
[22]D. E. Carlson and C. W. Magee, Appl. Phys. Lett. 33, 81 (1978).
[23]J. I. Pankove and D. E. Carlson, in *Proceedings of the Seventh International Conference on Amorphous and Liquid Semiconductors,* Ref. 21, p. 402.
[24]K. J. Matysik, C. J. Mogab and B. G. Bagley, J. Vac. Sci. Technol. 15, 302 (1978).
[25]D. K. Biegelsen, R. A. Street, C. C. Tsai, and J. C. Knights, Phys. Rev. B 20, 4839 (1979).
[26]J. A. Mc Millan and E. M. Pekison, Thin Solid Films 63, 189 (1979).
[27]P. A. Thomas, private communication.
[28]B. Bourdon, unpublished.
[29]E. Ligeon, A. Bontemps, J. Fontenille, and G. Guernet, in *Colloque International sur la Microélectronique Avancée, Paris, 1970,* edited by C. Chiron (Chiron, Paris, 1970), Tome 1, p. 50.

[30]E. Ligeon, A. Guivarch, J. Fontenille, M. Le Coutellec, R. Danielou, and J. Richard, Nucl. Instrum. Methods (in press).
[31]E. Ligeon, J. P. Bugeat, R. Danielou, J. Fontenille, and A. Guivarch, unpublished.
[32]E. Ligeon and A. Guivarch, Radiat. Eff. 22, 101 (1974).
[33]M. H. Brodsky, M. Cardona, and J. J. Cuomo, Phys. Rev. B 16, 3556 (1977).
[34]W. E. Spear and P. G. Lecomber, J. Non-Cryst. Solids 8-10, 727 (1972).
[35]K. Zellama, P. Germain, S. Squelard, J. C. Bourgoin, and P. A. Thomas, J. Appl. Phys. 50, 6995 (1979).
[36]*Encyclopedia of Chemistry*, 3rd ed., edited by Clifford A. Hampel and Gessner G. Hanely (Van Nostrand Reinhold, New York, 1973), p. 1001.
[37]K. Zellama, P. Germain, C. Picard, and B. Bourdon, unpublished.
[38]C. Kittel, Introduction à la Physique de l'Etat Solide, 3rd ed. (Dunod, Paris, 1972), p. 376.
[39]P. G. Lecomber and W. E. Spear, Phys. Rev. Lett. 25, 509 (1970).
[40]I. Solomon, T. Dietel, and D. Kaplan, J. Phys. (Paris) 39, 1241 (1978).
[41]D. L. Staebler and C. R. Wronski, Appl. Phys. Lett. 31, 292 (1977).
[42]A. Van Wieringen and N. Warmolitz, Physica 22, 849 (1956).
[43]H. Fritzsche, M. Tamelian, and C. C. Tsai, J. Appl. Phys. 50, 3366 (1979).
[44]R. Mosseri, Thèse de 3ème Cycle, l'Université Paris VII, 1979, unpublished.
[45]R. Fisch and D. C. Licciardello, Phys. Rev. Lett. 41, 889 (1978).
[46]Y. Adda and J. Philibert, *La Diffusion dans les Soildes*, 1st ed. (Presse Universitaire de France, Paris, 1966), Tome 1, p. 144.
[47]D. Dieumegard and D. Dubreuil, unpublished.
[48]P. Germain and K. Zellama, unpublished.